Engineering Solid Mechanics 2 (2014) 209-228

Contents lists available at GrowingScience

Engineering Solid Mechanics

homepage: www.GrowingScience.com/esm

Nonlinear forced vibration of hybrid composite rectangular plates

Alireza Shooshtari* **and Soheil Razavi**

Mechanical Engineering Department, Bu-Ali Sina University, 65175-4161 Hamedan, Iran

ARTICLE INFO

Article history:
Received January 20, 2014
Received in Revised form
April, 10, 2014
Accepted 14 April 2014
Available online
16 April 2014

Keywords:
Hybrid composites
Nonlinear forced vibration
Analytical modeling

ABSTRACT

In the present study, the nonlinear forced vibration of symmetric laminated rectangular plates, including Glare fiber metal laminated rectangular plate, is investigated based on the first order shear deformation theory. The boundary condition is considered to be immovable simply support. The Galerkin method is used to obtain the nonlinear ordinary differential equation in terms of an unknown time function. The obtained equation is solved analytically by the multiple time scales method. The obtained results are compared with the numerical solution of the nonlinear ordinary differential equation of motion and a good agreement is found between them.

1. Introduction

The composite materials are good alternatives to metals because of their low weight, high strength and stiffness, and environmental resistance. Fiber metal laminates (FMLs) are hybrid materials comprising interleaved metal sheets and fiber-reinforced polymer layers. They were developed as lightweight alternatives to structural metals (Langdon et al., 2009). One of the advantages of FML materials when compared with conventional carbon fiber/epoxy composites is the low moisture absorption, due to the barrier of the outer aluminum layers (Botelho et al., 2006). The only commercially used FML is Glare, which comprises thin aluminum sheets and glass-fiber-reinforced epoxy. Although the initial use of Glare in aircraft was to improve the fatigue properties of aircraft components, Glare has also been used because of its improved impact properties, relative to aluminum of the same areal density. Presently, there is a motivation in the aerospace industry to produce lighter aircraft, as the costs of fuel increase. Glare is currently used as a material in the upper fuselage and leading edges of the Airbus A380 (Langdon et al., 2009).

* Corresponding author. Tel.: +98 8118272410
E-mail addresses: shooshta@basu.ac.ir (A. Shooshtari)

doi: 10.5267/j.esm.2014.4.002

Nowadays, Glare materials are commercialized in six different standard grades; for the Glare 1, Glare 2, Glare 4 and Glare 5 the composite laminae are stacked symmetrically. In the case of Glare 3 composite, the composite lamina have a cross-ply fiber layer stacked to the nearest outer aluminum layer of the laminate, in relation to the rolling direction of the aluminum. For the Glare 6 composite, the composite layers are stacked at + 45° and – 45° (Botelho et al., 2006).

Rashidi et al. (2012) used homotopy perturbation method to study the nonlinear free vibration of rectangular isotropic plates. Zhang and Zhao (2012) investigated the nonlinear vibrations of a composite laminated cantilever rectangular plate subjected to thin-plane and transversal excitations. They used Reddy's third-order plate theory along with Galerkin method to obtain the equations of motion and used the method of multiple scales to solve these equations. Asymptotic numerical method is used to study the nonlinear forced vibration of thin isotropic rectangular plates by Boumediene et al. (2009). Wei et al. (2012) studied the nonlinear free vibration of hybrid composite plate with an initial stress on elastic foundations. They used Mindlin plate theory to model the problem and after implementing the Galerkin method to reduce the governing nonlinear partial differential equations to ordinary nonlinear differential equations, they employed the Runge–Kutta method to obtain the nonlinear frequencies.

Ribeiro (2004) used the hybrid finite element method (HFEM) based on the first order shear deformation theory to study nonlinear forced vibration of isotropic beams and plates. Amabili(2004) investigated nonlinear forced vibration of isotropic rectangular plates numerically. Ribeiro (2005) studied the nonlinear forced vibration of simply supported rectangular plates and obtained the backbone curves and the nonlinear mode shapes for three first modes. Abe et al. (1998) studied the sub-harmonic resonance of moderately thick anti-symmetric angle-ply laminated rectangular plates by using the multiple scales method. Ribeiro (2006) studied the nonlinear forced vibration of laminated rectangular, taking into account the rotary inertia term and transverse shear deformation. Singha and Daripa (2009) used the finite element method for studying nonlinear forced vibration of composite rectangular plates. Amabili and Farhadi (2009) studied nonlinear forced vibration of simply supported rectangular plates and laminated plates by using Lagrange method. Harras et al. (2004) investigated the linear and nonlinear dynamic of a five-layered Glare 3 rectangular plate both experimentally and theoretically. Shooshtari and Razavi (2010) investigated linear and nonlinear free vibration of laminated and FML rectangular plates.

It is seen that in most of the published papers, the obtained equations are solved numerically. Moreover, there is not sufficient study about the nonlinear forced vibration of Glare rectangular plates. Thus, it is needed to find an analytical relation for the frequency response of laminated composite and Glare rectangular plates in order to determine the effects of various lamination and plate parameters on the steady-state motion in the primary and secondary resonances.

In the present study, the nonlinear forced vibration in the primary and secondary resonances is investigated. The analytical relations of the frequency response equations in the steady-state motion are obtained by using the multiple time scales method. The present procedure is only valid for finite amplitude vibrations. The effects of layup scheme, aspect ratio, moduli ratio, length-to-thickness ratio, and number of layers on the frequency responses of symmetric laminated and Glare FML rectangular plates are studied. The nonlinear forced vibration of various grades of Glare rectangular plates is also investigated.

2. Formulation of nonlinear differential equation of motion in the forced vibration case

Equations of motion of rectangular plates, based on the first order shear deformation theory are (Reddy, 2004):

$$N_{x,x} + N_{xy,y} = I_0 u_{0,tt} + I_1 \phi_{x,tt} \tag{1}$$

$$N_{xy,x} + N_{y,y} = I_0 v_{0,tt} + I_1 \phi_{y,tt} \tag{2}$$

$$Q_{x,x} + Q_{y,y} + \mathcal{N}(w_0) + q = I_0 w_{0,tt} \tag{3}$$

$$M_{x,x} + M_{xy,y} - Q_x = I_2 \phi_{x,tt} + I_1 u_{0,tt} \tag{4}$$

$$M_{xy,x} + M_{y,y} - Q_y = I_2 \phi_{y,tt} + I_1 v_{0,tt} \tag{5}$$

where subscript ',' denotes partial differentiation with respect to the following parameter (or parameters).u_0, v_0, and w_0 are the displacements of a material point on the mid-surface along $x-$, $y-$, and $z-$axes, respectively. $\phi_x$andϕ_y are the rotations of a transverse normal about the $y-$ and $x-$axes, respectively. N_x, N_y, and N_{xy} are the in-plane force resultants,Q_x and Q_y are the transverse force resultants, M_x, M_y, and M_{xy} are the moments resultants and I_0, I_1, and I_2 are the mass moments of inertia. $q$is the applied transverse force which is harmonic in time (i.e., $q = q_0 \cos(\Omega t)$), with q_0 and Ωhaving constant values. $\mathcal{N}(w_0)$is in the following form:

$$\mathcal{N}(w_0) = \left(N_x w_{0,x} + N_{xy} w_{0,y}\right)_{,x} + \left(N_{xy} w_{0,x} + N_y w_{0,y}\right)_{,y} \tag{6a}$$

The immovable boundary condition is expressed by:

$$\begin{aligned} &w = w_{,xx} = \psi_{,xy} = u_0 = 0 \quad (x = 0, a) \\ &w = w_{,yy} = \psi_{,xy} = v_0 = 0 \quad (y = 0, b) \end{aligned} \tag{6b}$$

whereψ is force function and defined by:

$$N_x = \psi_{,yy}, \quad N_y = \psi_{,xx}, \quad N_{xy} = -\psi_{,xy}. \tag{7}$$

Assuming the density of plate material (ρ_0) as an even function of thickness (z) and neglecting in-plane inertia effects ($u_{0,tt}$ and $v_{0,tt}$), Eq. (1) to Eq. (5) reduce to the following equations, which are written in terms of the displacements and the force function:

$$K\left[A_{44}\left(w_{,yy} + \varphi_{y,y}\right) + A_{55}\left(w_{,xx} + \varphi_{x,x}\right)\right] + \psi_{,yy} w_{,xx} + \psi_{,xx} w_{,yy} - 2\psi_{,xy} w_{,xy} + q_0 \cos \Omega t = I_0 \ddot{w}, \tag{8}$$

$$D_{11}\varphi_{x,xx} + D_{12}\varphi_{y,xy} + D_{66}\left(\varphi_{x,yy} + \varphi_{y,xy}\right) - KA_{55}\left(w_{,x} + \varphi_x\right) = I_2 \ddot{\varphi}_x, \tag{9}$$

$$D_{12}\varphi_{x,xy} + D_{22}\varphi_{y,yy} + D_{66}\left(\varphi_{x,xy} + \varphi_{y,xx}\right) - KA_{44}\left(w_{,y} + \varphi_y\right) = I_2 \ddot{\varphi}_y. \tag{10}$$

Along with a compatibility equation in the following form (Chia, 1980):

$$A_{22}^* \psi_{,xxxx} + (2A_{12}^* + A_{66}^*)\psi_{,xxyy} + A_{11}^* \psi_{,yyyy} = w_{,xy}^2 - w_{,xx} w_{,yy}, \tag{11}$$

where K is the shear correction factor,$A_{ij}$is the component of extensional stiffness matrix, and$D_{ij}$is the component of bending stiffness matrix. The constant coefficients of Eq. (11) are obtained by:

$A_{11}^* = A_{22}(A_{11}A_{22} - A_{12}^2)^{-1}$, $A_{12}^* = -A_{12}(A_{11}A_{22} - A_{12}^2)^{-1}$, $A_{22}^* = A_{11}(A_{11}A_{22} - A_{12}^2)^{-1}$, $A_{66}^* = (A_{66})^{-1}$(Chia, 1980).

Eq. (9) and Eq. (10) lead to a set of equations with two unknown parameters which areφ_x and φ_y. This set of equations gives $\varphi_x$and φ_y in the following form:

$$\phi_x = \left[\frac{KA_{55}\frac{\partial}{\partial x}\left(D_{66}\frac{\partial^2}{\partial x^2}+D_{22}\frac{\partial^2}{\partial y^2}-I_2\frac{\partial^2}{\partial t^2}-KA_{44}\right)-KA_{44}\frac{\partial}{\partial y}\left((D_{12}+D_{66})\frac{\partial^2}{\partial x\partial y}\right)}{\left(D_{11}\frac{\partial^2}{\partial x^2}+D_{66}\frac{\partial^2}{\partial y^2}-I_2\frac{\partial^2}{\partial t^2}-KA_{55}\right)\left(D_{66}\frac{\partial^2}{\partial x^2}+D_{22}\frac{\partial^2}{\partial y^2}-I_2\frac{\partial^2}{\partial t^2}-KA_{44}\right)-K^2A_{44}A_{55}\frac{\partial^2}{\partial x\partial y}}\right]w \quad (12a)$$

$$\phi_y = \left[\frac{KA_{44}\frac{\partial}{\partial y}\left(D_{11}\frac{\partial^2}{\partial x^2}+D_{66}\frac{\partial^2}{\partial y^2}-I_2\frac{\partial^2}{\partial t^2}-KA_{55}\right)-KA_{55}\frac{\partial}{\partial x}\left((D_{12}+D_{66})\frac{\partial^2}{\partial x\partial y}\right)}{\left(D_{11}\frac{\partial^2}{\partial x^2}+D_{66}\frac{\partial^2}{\partial y^2}-I_2\frac{\partial^2}{\partial t^2}-KA_{55}\right)\left(D_{66}\frac{\partial^2}{\partial x^2}+D_{22}\frac{\partial^2}{\partial y^2}-I_2\frac{\partial^2}{\partial t^2}-KA_{44}\right)-K^2A_{44}A_{55}\frac{\partial^2}{\partial x\partial y}}\right]w \quad (12b)$$

Substituting the obtained φ_x and φ_y into Eq. (8) gives the following nonlinear partial differential equation in terms of w and ψ:

$$\begin{aligned}\Big\{K\Big[&A_{55}\frac{\partial}{\partial x}(L_2^*L_6^*-L_3^*L_5^*)+A_{44}\frac{\partial}{\partial y}(L_3^*L_4^*-L_1^*L_6^*)+\left(A_{55}\frac{\partial^2}{\partial x^2}+A_{44}\frac{\partial^2}{\partial y^2}\right)(L_2^*L_4^*-L_1^*L_5^*)\Big]\\&+\left(\frac{\partial^2\psi}{\partial y^2}\frac{\partial^2}{\partial x^2}+\frac{\partial^2\psi}{\partial x^2}\frac{\partial^2}{\partial y^2}-2\frac{\partial^2\psi}{\partial x\partial y}\frac{\partial^2}{\partial x\partial y}-I_0\frac{\partial^2}{\partial t^2}\right)(L_2^*L_4^*-L_1^*L_5^*)\Big\}w\\&+(L_2^*L_4^*-L_1^*L_5^*)q_0\cos\Omega t=0\end{aligned} \quad (13)$$

where $L_i^*(i=1,\dots,6)$ are the partial differential operators and are given in Appendix A. w and ψ for the immovable simply-supported boundary condition can be written in the form of (Chia, 1980):

$$w = hf(t)\sin\left(\frac{\pi x}{a}\right)\sin\left(\frac{\pi y}{b}\right), \quad (14)$$

$$\psi = k_1x^2+k_2y^2+\frac{h^2f^2(t)}{32}\left\{\frac{(a/b)^2}{A_{22}^*}\cos\left(\frac{2\pi x}{a}\right)+\frac{(b/a)^2}{A_{11}^*}\cos\left(\frac{2\pi y}{b}\right)\right\},$$

$$k_1 = -\frac{h^2f^2(t)}{16}\left[\left(\frac{\pi}{a}\right)^2A_{12}^*-\left(\frac{\pi}{b}\right)^2A_{11}^*\right]\left(A_{11}^*A_{22}^*-{A_{12}^*}^2\right)^{-1}, \quad (15)$$

$$k_2 = \frac{h^2f^2(t)}{16}\left[\left(\frac{\pi}{a}\right)^2A_{22}^*-\left(\frac{\pi}{b}\right)^2A_{12}^*\right]\left(A_{11}^*A_{22}^*-{A_{12}^*}^2\right)^{-1},$$

where a, b, and h are the length, width, and thickness of the plate, respectively and $f(t)$ is an unknown time function.

The Galerkin method is applied by using $\iint_A L\cdot w dxdy=0$, in which A is the area of the rectangular plate and L is the left hand of Eq. (13). This transforms the nonlinear partial differential equation of Eq. (13) to the following nonlinear ordinary differential equation in terms of the unknown time function:

$$Z_1\ddot{f}+Z_2f+Z_3f^3+Z_4\ddot{f}f^2+Z_5\dot{f}^2f=\hat{q}\cos(\Omega t). \quad (16)$$

where $\hat{q}=[I_2\Omega^2K(A_{44}+A_{55})-K^2A_{44}A_{55}]q_0$, and $Z_i(i=1,\dots,5)$ are constant coefficients which are functions of plate parameters (i.e., length, width, thickness, and density) and stiffness components. These coefficients are obtained in terms of plate parameters and stiffness components, and are given in Appendix B, in which it is seen that $Z_5=2Z_4$.

According to Appendix B, the units of Z_1, Z_4, and Z_5 are kg^3mms^{-4}, while the units of Z_2 and Z_3 are kg^3mms^{-6}. Since the coefficients of $\ddot{f}$, $\ddot{f}f^2$, and $\dot{f}^2f$ are from the same dimension,all of them are inertia terms. On the other hand, $\ddot{f}f^2$ and $\dot{f}^2f$ are nonlinear terms. Therefore, $\ddot{f}f^2$ and $\dot{f}^2f$ are called nonlinear inertia terms.

Adding on the viscous damping effect (Abe et al. 1998) and assuming the dimensionless time to be in the form of $\tau=\frac{1}{a^2}\sqrt{\Lambda}t$,the dimensionless form of Eq. (16) is:

$$f_{,\tau\tau} + 2\xi\omega f_{,\tau} + \omega^2 f + \alpha_1^2 f^3 + \beta_1^2 f_{,\tau\tau} f^2 + \gamma_1^2 f_{,\tau}^2 f = Q\cos(\Omega\bar{\Lambda}\tau), \quad (17)$$

where ξ is the damping ratio, ω is the dimensionless natural frequency, α_1^2 is the coefficient of nonlinear stiffness term because it only contains stiffness components, and β_1^2 and γ_1^2 are the coefficients of nonlinear inertia terms because they contain density term in addition to stiffness components. It is simply noticed from Eq. (16) and Eq. (17) that, $\beta_1^2 = Z_4/Z_1$, and $\gamma_1^2 = Z_5/Z_1$.Considering $Z_5 = 2Z_4$, it is obtained that $\gamma_1^2 = 2\beta_1^2$ which is utilized throughout the paper.

For cross-ply laminated rectangular plates,$\Lambda = (E_2 h^2/\rho_0)$, and for the FML plates,$\Lambda = D_{11}^*/I_0$ are defined (Shooshtari & Razavi, 2010).The other unknown parameters of Eq. (17) are defined by following equation:

$$Q = [a^4\hat{q}]/(Z_1\Lambda), \quad \bar{\Lambda} = a^2/\sqrt{\Lambda}. \quad (18)$$

The present method is only valid for finite amplitude vibrations, since in large amplitude vibrations even combination or internal resonances can occur at excitation frequencies other than $\Omega = \omega_{11}$.

3. Primary resonance

3.1 Solution of the primary resonance by using the method of multiple scales

In the primary resonance, excitation force and nonlinear terms are of the same order (Nayfeh &Mook, 1995). So if the small, positive and dimensionless parameter ε is taken to be $(h/a)^2$(Shooshtari & Razavi, 2010), Eq. (17) is rewritten in the following form:

$$f_{,\tau\tau} + \omega^2 f + \varepsilon\left(2\mu f_{,\tau} + \alpha^2 f^3 + \beta^2 f_{,\tau\tau} f^2 + \gamma^2 f_{,\tau}^2 f - \hat{Q}\cos(\Omega\bar{\Lambda}\tau)\right) = 0, \quad (19)$$

where $\alpha^2 = \alpha_1^2 \times (a/h)^2$, $\beta^2 = \beta_1^2 \times (a/h)^2$, $\gamma^2 = \gamma_1^2 \times (a/h)^2$, $\hat{Q} = Q/\varepsilon$, and $\mu = \xi\omega/\varepsilon$.
In the primary resonance, a detuning parameterσ, which is used to show the nearness of natural frequency to excitation frequency, is defined as (Nayfeh & Mook, 1995):

$$\Omega = \omega_0 + \varepsilon\sigma \quad (20)$$

where ω_0 is the circular natural frequency in rads^{-1}.

Substituting Eq. (20) into Eq. (19) results in

$$f_{,\tau\tau} + \omega^2 f + \varepsilon\left(2\mu f_{,\tau} + \alpha^2 f^3 + \beta^2 f_{,\tau\tau} f^2 + \gamma^2 f_{,\tau}^2 f - \hat{Q}\cos(\omega T_0 + \bar{\Lambda}\sigma T_1)\right) = 0, \quad (21)$$

where T_0 and T_1 are independent time variables and are defined by Nayfeh and Mook (1995):

$$T_n = \varepsilon^n \tau \quad for \quad n = 0,1,\ldots \quad (22)$$

f can be writtenin the following form:

$$f(\tau;\varepsilon) = f_0(T_0, T_1) + \varepsilon f_1(T_0, T_1) + \cdots \quad (23)$$

The derivatives with respect to τ can be written in terms of partial derivatives of T_n according to:

$$\frac{d}{d\tau} = D_0 + \varepsilon D_1,$$
$$\frac{d^2}{d\tau^2} = D_0^2 + 2\varepsilon D_0 D_1, \quad (24)$$

where D_0 and D_1 denote $\partial/\partial T_0$ and $\partial/\partial T_1$, respectively.

Substituting Eq. (23) and Eq. (24) into Eq. (21) and equating the coefficients of ε^0 and ε^1 to zero, gives:

$$D_0^2 f_0 + \omega^2 f_0 = 0, \tag{25}$$

$$D_0^2 f_1 + \omega^2 f_1 = -2D_0 D_1 f_0 - 2\mu D_0 f_0 - \alpha^2 f_0^3 - \beta^2 f_0^2 (D_0^2 f_0) - \gamma^2 f_0 (D_0 f_0)^2 + \hat{Q}\cos[\omega T_0 + \bar{\Lambda}\sigma T_1]. \tag{26}$$

General solution of Eq. (25) is:

$$f_0 = A_2(T_1)\exp(i\omega T_0) + cc, \tag{27}$$

where A_2 is an unknown complex function of T_1 and *cc* denotes the complex conjugate of the preceding terms.

Substituting Eq. (27) into Eq. (26) and by using the complex form of $\hat{Q}\cos[\omega T_0 + \bar{\Lambda}\sigma T_1]$, Eq. (26) becomes:

$$\begin{aligned} D_0^2 f_1 + \omega^2 f_1 = \Big[& -2i\omega A_2' - 3A_2^2 \bar{A}_2 \alpha^2 - 2i\omega\mu A_2 + \omega^2 A_2^2 \bar{A}_2 \beta^2 \\ & + \tfrac{1}{2}\hat{Q}\exp(i\bar{\Lambda}\sigma T_1)\Big]\exp(i\omega T_0) + (3\omega^2\beta^2 - \alpha^2)A_2^3\exp(3i\omega T_0) + cc, \end{aligned} \tag{28a}$$

where superscript ($'$) denotes $\partial/\partial T_1$. Coefficients of $\exp(i\omega T_0)$, which are called secular terms, lead to non-periodic solution. In order to have a periodic solution, the secular terms must be equated to zero:

$$\left[-2i\omega A_2' - 3A_2^2 \bar{A}_2 \alpha^2 - 2i\omega\mu A_2 + \omega^2 A_2^2 \bar{A}_2 \beta^2 + \tfrac{1}{2}\hat{Q}\exp(i\bar{\Lambda}\sigma T_1)\right] = 0. \tag{28b}$$

Eq. (28b) is called the solvability condition.

If A_2 is defined in the polar form of (i.e.,$A_2 = \frac{1}{2}r\exp(is)$ and is substituted in the solvability condition, first approximation of f can be written in the following form:

$$f = r\cos(\omega\tau + s) + O(\varepsilon), \tag{29}$$

where the amplitude (r) and phase (s) are obtained by:

$$r' = -\mu r + \frac{\hat{Q}}{2\omega}\sin(\bar{\Lambda}\sigma T_1 - s), \tag{30a}$$

$$rs' = \frac{1}{8}\left(\frac{3}{\omega}\alpha^2 - \omega\beta^2\right)r^3 - \frac{\hat{Q}}{2\omega}\cos(\bar{\Lambda}\sigma T_1 - s). \tag{30b}$$

For an autonomous system, by defining $\eta = \bar{\Lambda}\sigma T_1 - s$, Eq. (30a) and Eq. (30b) are transformed to:

$$r' = -\mu r + \frac{\hat{Q}}{2\omega}\sin\eta, \tag{31a}$$

$$r\eta' = r\sigma\bar{\Lambda} - \frac{1}{8}\left(\frac{3}{\omega}\alpha^2 - \omega\beta^2\right)r^3 + \frac{\hat{Q}}{2\omega}\cos\eta. \tag{31b}$$

3.2 Steady-state motion

Steady-state motion occurs when $r' = \eta' = 0$, which corresponds to the singular points of Eq. (31a) and Eq. (31b) (Nayfeh & Mook, 1995). Thus:

$$\mu r = \frac{\hat{Q}}{2\omega}\sin\eta, \tag{32a}$$

$$-r\sigma\bar{\Lambda} + \frac{1}{8}\left(\frac{3}{\omega}\alpha^2 - \omega\beta^2\right)r^3 = \frac{\hat{Q}}{2\omega}\cos\eta. \tag{32b}$$

Squaring and adding Eq. (32a) and Eq. (32b) gives the frequency response equation:

$$\left[\mu^2 + \left(\frac{1}{8}P_1 r^2 - \sigma\bar{\Lambda}\right)^2\right]r^2 = \frac{\hat{Q}^2}{4\omega^2}, \tag{33}$$

where $P_1 = \frac{3\alpha^2 - \beta^2\omega^2}{\omega}$.

4. Secondary resonance

In the secondary resonance, the amplitude of excitation is hard (Nayfeh and Mook, 1995). So Eq. (17) is transformed to:

$$f_{,\tau\tau} + \omega^2 f + \varepsilon\left(2\mu f_{,\tau} + \alpha^2 f^3 + \beta^2 f_{,\tau\tau} f^2 + \gamma^2 f_{,\tau}^2 f\right) = Q\cos(\Omega\bar{\Lambda}\tau) \tag{34}$$

Substituting Eq. (23) into Eq. (34) and equating the coefficients of ε^0 and ε^1 on both sides, it is obtained that:

$$D_0^2 f_0 + \omega^2 f_0 = Q\cos(\Omega\bar{\Lambda}\tau), \tag{35}$$

$$D_0^2 f_1 + \omega^2 f_1 = -2D_0 D_1 f_0 - 2\mu D_0 f_0 - \alpha^2 f_0^3 - \beta^2 f_0^2 (D_0^2 f_0) - \gamma^2 f_0 (D_0 f_0)^2. \tag{36}$$

Complete solution of Eq. (35) is:

$$f_0 = A_2(T_1)\exp(i\omega T_0) + \tilde{Q}\exp(i\Omega\bar{\Lambda}T_0) + cc \tag{37}$$

where $\tilde{Q} = \frac{1}{2}Q[\omega^2 - (\Omega\bar{\Lambda})^2]^{-1}$.

Substituting Eq. (37) into Eq. (36), results in two cases of secondary resonance depending on the definition of detuning parameter. That is, the secondary resonance may be either super-harmonic or sub-harmonic depending on the definition of the detuning parameter.

4.1. Super-harmonic resonance

In the super-harmonic resonance, the detuning parameter is defined by$3\Omega = \omega_0 + \varepsilon\sigma$. So the solvability condition of Eq. (36) becomes:

$$\beta^2\omega^2\left(A_2^2\bar{A}_2 + 2\tilde{Q}^2 A_2\right) - \left(3\alpha^2 A_2^2\bar{A}_2 + 6\alpha^2 A_2\tilde{Q}^2 + 2i\omega A_2' + 2i\omega\mu A_2\right) + [3\beta^2(\Omega\bar{\Lambda})^2 - \alpha^2]\tilde{Q}^3\exp(i\bar{\Lambda}\sigma T_1) = 0. \tag{38}$$

Substituting $A_2 = \frac{1}{2}r\exp(is)$ into Eq. (38) gives:

$$r' = -\mu r + \frac{3\beta^2(\Omega\bar{\Lambda})^2 - \alpha^2}{\omega}\tilde{Q}^3\sin(\bar{\Lambda}\sigma T_1 - s), \tag{39}$$

$$rs' = \frac{3\alpha^2-\beta^2\omega^2}{\omega}\left(\tilde{Q}^2+\frac{1}{8}r^2\right)r - \frac{3\beta^2(\Omega\bar{\Lambda})^2-\alpha^2}{\omega}\tilde{Q}^3\cos(\bar{\Lambda}\sigma T_1 - s). \tag{40}$$

Defining a new parameter as $\eta = \bar{\Lambda}\sigma T_1 - s$ results in:

$$r' = -\mu r + \frac{3\beta^2(\Omega\bar{\Lambda})^2-\alpha^2}{\omega}\tilde{Q}^3\sin\eta, \tag{41a}$$

$$r\eta' = r\sigma\bar{\Lambda} - \frac{3\alpha^2-\beta^2\omega^2}{\omega}\left(\tilde{Q}^2+\frac{1}{8}r^2\right)r + \frac{3\beta^2(\Omega\bar{\Lambda})^2-\alpha^2}{\omega}\tilde{Q}^3\cos\eta. \tag{41b}$$

In the steady-state motion Eq. (41a) and Eq. (41b) are changed to:

$$\mu r = \frac{3\beta^2(\Omega\bar{\Lambda})^2-\alpha^2}{\omega}\tilde{Q}^3\sin\eta \tag{42a}$$

$$-r\sigma\bar{\Lambda} + \frac{3\alpha^2-\beta^2\omega^2}{\omega}\left(\tilde{Q}^2+\frac{1}{8}r^2\right)r = \frac{3\beta^2(\Omega\bar{\Lambda})^2-\alpha^2}{\omega}\tilde{Q}^3\cos\eta \tag{42b}$$

from which the frequency response equation is obtained:

$$\left[\mu^2 + \left[P_1\tilde{Q}^2 + \frac{1}{8}P_1r^2 - \sigma\bar{\Lambda}\right]^2\right]r^2 = P_2\tilde{Q}^6 \tag{43}$$

where$P_2 = \left[\frac{3\beta^2(\Omega\bar{\Lambda})^2-\alpha^2}{\omega}\right]^2$.

4.2. Sub-harmonic resonance

In the sub-harmonic resonance, the detuning parameter is defined by $\Omega = 3\omega_0 + \varepsilon\sigma$, which gives the following solvability condition:

$$\beta^2\omega^2\left(A_2^2\bar{A}_2 + 2\tilde{Q}^2A_2\right) - \left(3\alpha^2A_2^2\bar{A}_2 + 6\alpha^2A_2\tilde{Q}^2 + 2i\omega A_2' + 2i\omega\mu A_2\right) - [3\alpha^2 + \beta^2(4\omega\Omega\bar{\Lambda} - 4\omega^2 - (\Omega\bar{\Lambda})^2)]\tilde{Q}\bar{A}_2^2\exp(i\bar{\Lambda}\sigma T_1) = 0. \tag{44}$$

By a similar procedure which is introduced in the primary and the super-harmonic resonances, the following equations for free vibration amplitude(r) and phase(η) of an autonomous system are obtained:

$$r' = -\mu r + \frac{P_3\tilde{Q}}{4\omega}r^2\sin\eta, \tag{45a}$$

$$r\eta' = r\sigma\bar{\Lambda} - 3P_1\left(\tilde{Q}^2+\frac{1}{8}r^2\right)r + \frac{3P_3\tilde{Q}}{4\omega}r^2\cos\eta, \tag{45b}$$

where $P_3 = -3\alpha^2 - \beta^2[4\omega\Omega\bar{\Lambda} - 4\omega^2 - (\Omega\bar{\Lambda})^2]$.

Eq. (45a) and (45b) give the frequency response equation:

$$9\mu^2 + \left[\sigma\bar{\Lambda} - 3P_1\tilde{Q}^2 - \frac{3}{8}P_1r^2\right]^2 = \left(\frac{3P_3\tilde{Q}}{4\omega}\right)^2 r^2 \tag{46}$$

5. Numerical study

The determination of the shear correction coefficient K for laminated structures is still an unresolved issue (Reddy, 2004). For moderately thick $(a/h \geq 10)$ laminated plates $K = 5/6$ gives fairly accurate results (Ribeiro, 2009). So, due to the thinness of the analyzed plates in this paper, $K = 5/6$ is used in the frequency response equations.

In this study, Ω is approximated to ω_0, $\frac{1}{3}\omega_0$, and $3\omega_0$ in primary, super-harmonic, and sub-harmonic resonances, respectively. This is approved by Fig. 1 for a five-layered Glare 3 square plate in the primary and secondary resonances, where the dimensionless excitation amplitude ($f_i = \frac{q_0 a}{E_2 h}$) is taken to be 56. It is noticed that, because the curves are too similar, the pictures do not succeed in showing the difference. So the proposed approximation of Ωare acceptable.

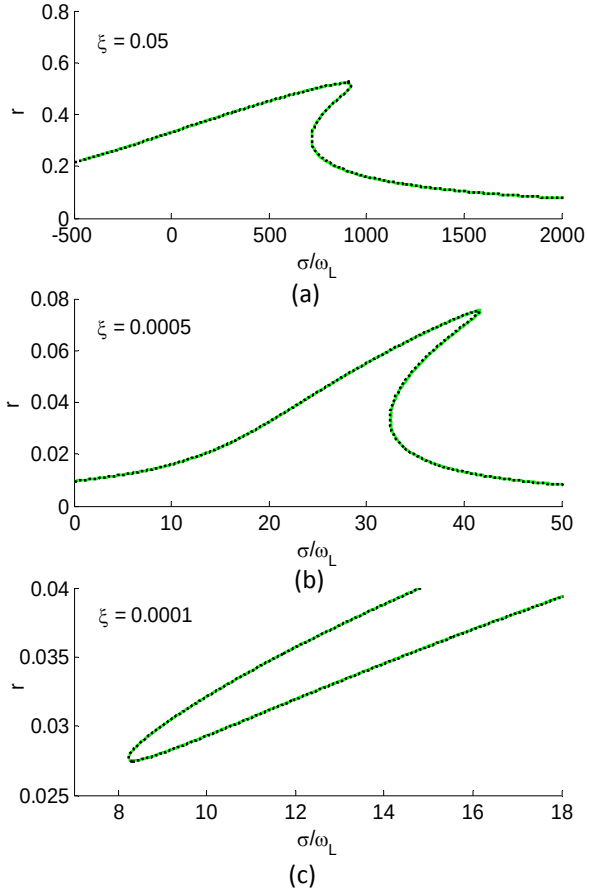

Fig. 1. Comparison of exact and approximate frequency response curves of a five-layered square Glare 3 plate in the: (a) primary resonance, (b) super-harmonic resonance, and (c) sub-harmonic resonance; ——— exact frequency response curve, -------- approximate frequency response curve

The total thickness and length of plates are taken to be 1 mm and 100 mm, respectively. The thicknesses of aluminum sheets and each fiber-reinforced layer of studied FML rectangular plates are given in Table 1. Table 2 gives the material properties of studied plates.

Table 1. Glare grades studied in this paper (Botelho et al., 2006)

Glare grade	Al sheet thickness (mm)	Each fiber layer thickness (mm)	Prepared orientation in each fiber layer	Main characteristic
Glare 2B	0.3 (2024-T3)	0.1	90°/90°	fatigue, strength
Glare 3	0.3 (2024-T3)	0.1	0°/90°	fatigue, impact
Glare 4B	0.7/3 (2024-T3)	0.1	90°/0°/90°	fatigue, strength in 0^o direction
Glare 5	0.2 (2024-T3)	0.1	0°/90°/90°/0°	shear, off-axis properties

Table 2. Material properties of the aluminum alloy (Botelho et al., 2006) and GFRC (Lu & Li, 2009)

Materials	E (GPa)	G (GPa)	ρ_0 (kgm^{-3})	ν
Aluminum alloy 2024-T3	72.4	28	2700	0.33
GFRC	$E_1 = 55.8979$ $E_2 = 13.7293$	$G_{12} = 5.5898$ $G_{13} = 5.5898$ $G_{23} = 4.9033$	2550	0.277

5.1 Primary resonance

To verify the accuracy of the proposed method, the frequency response curve of an isotropic square plate in the primary resonance is obtained and compared with the published results (Fig. 2).

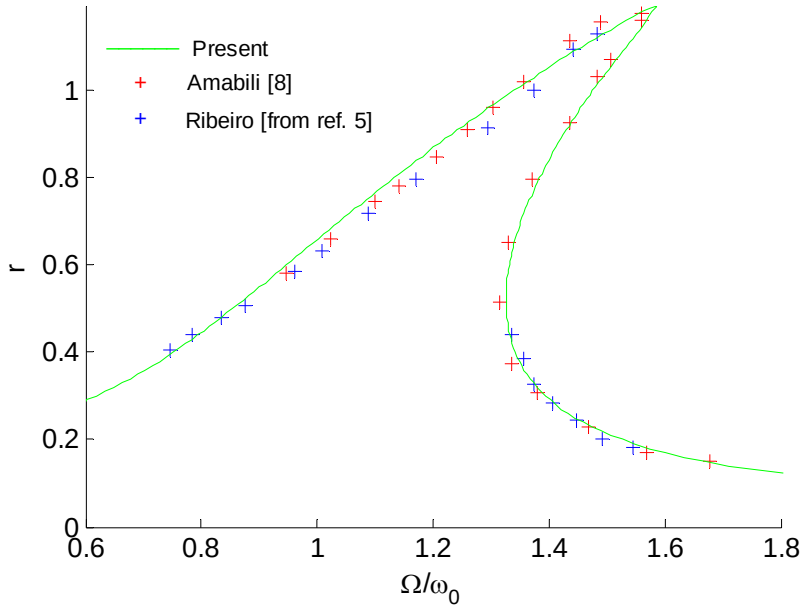

Fig. 2. Frequency response curve of an isotropic square plate by using several methods

It is seen that there is an acceptable agreement between the results of the present approach and the published ones. The variations of dimensionless amplitude of motion with respect to excitation frequency (i.e., the frequency response curve) of a laminated square GFRC plate with different number of layers and layup is studied and the results are shown in Fig. 3, where it is seen that there is a very small different between these curves. Eq. (47), which is obtained by using Eq. (33), verifies this claim.

$$\sigma = 359266.829r^2 \pm 13812.172[(q_0/r)^2 - 67.378]^{1/2} \text{for} \quad [0^\circ/90^\circ/0^\circ]$$

$$\sigma = 359289.571r^2 \pm 13811.493[(q_0/r)^2 - 67.390]^{1/2} \text{ for} \quad [0^\circ/90^\circ/0^\circ/90^\circ/0^\circ] \tag{47}$$

$$\sigma = 359291.189r^2 \pm 13811.387[(q_0/r)^2 - 67.391]^{1/2} \text{ for} \quad [0^\circ/90^\circ/90^\circ/90^\circ/0^\circ]$$

It is also seen that the responses of $[0^\circ/90^\circ/0^\circ]$ and $[0^\circ/90^\circ/0^\circ/90^\circ/0^\circ]$are the same as those of $[90^\circ/0^\circ/90^\circ]$ and $[90^\circ/0^\circ/90^\circ/0^\circ/90^\circ]$ layups, respectively.

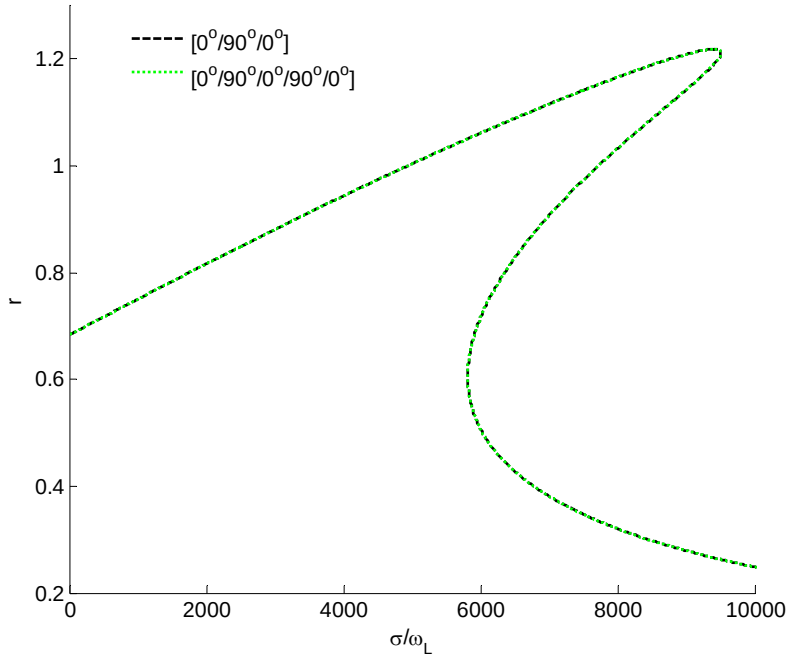

Fig. 3. Frequency response curve of a laminated GFRC square plate for different lamination schemes with dimensionless excitation amplitude being 72.8 and $\xi = 0.2$

The effects of excitation amplitude and aspect ratio on the frequency response curve of a rectangular plate are studied and the results are shown for a five-layered rectangular Glare 3 plate in Figs. 4(a) and 4(b), respectively. Although for higher excitation amplitudes, the maximum amplitude of motion (r) increases, there is not any change in the degree of hardening nonlinearity. It is also seen that higher aspect ratios result in smaller amplitudes of motion. The frequency responses of five-layered Glare 3, GFRC, Glare 2B, and Glare 4Bsquare plates are studied and the resulted curves are shown in Figs. 4(c) and 4(d). It is observed that for GFRC plate, amplitude of motion is bigger than that of the Glare 3 plate and the degree of hardening nonlinearity is a little higher for the GFRC plate. This arises from the fact that the used aluminum sheets in Glare plates have higher elasticity module compared with GFRC layers, which simply results in lower transverse deflection in Glare plates. Fig. 4(d) shows that the frequency responses of Glare 3 and Glare 2B plates are almost the same, where the amplitude of motion for the Glare 4B plate increases with higher rate compared with those of the Glare 2B and Glare 3 plates. The layups of studied Glare 2B, Glare 3, and Glare 4B plates are in the following form, respectively (Botelho et al., 2006):

Al (2024-T3) / [90°/90°] GFRC / Al (2024-T3) / [90°/90°] GFRC / Al (2024-T3),

Al(2024-T3) / [0°/90°] GFRC / Al (2024-T3) / [90°/0°] GFRC / Al (2024-T3),

Al (2024-T3) / [90°/0°/90°] GFRC / Al (2024-T3) / [90°/0°/90°] GFRC / Al (2024-T3).

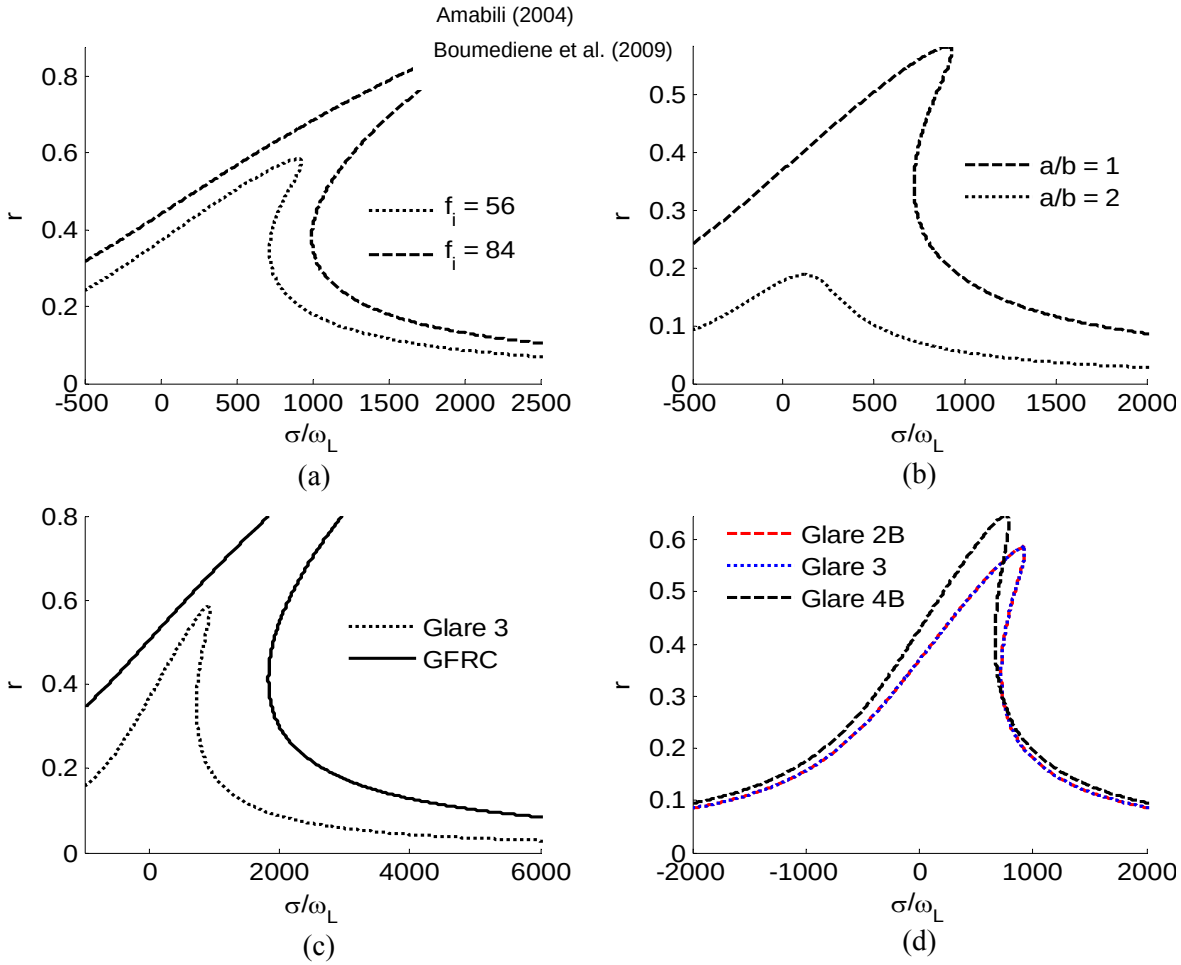

Fig. 4. Frequency response curve of: (a) a five-layered square Glare 3 for two excitation amplitudes, (b) a five-layered Glare 3 panel for two aspect ratios ($f_i = 56$), (c) two types of five-layered square plates ($f_i = 56$), and (d) three grades of five-layered square Glare plates ($f_i = 56$), for $\xi = 0.05$

This is obvious from the layups of Glare plates, that the responses of Glare 2B and Glare 3 are nearly the same, but because the ratio of the GFRC layers is less in Glare 4B, the amplitude of motion is increased comparing with those of the Glare 2B and Glare 3 plates. The effects of length-to-thickness ratio (a/h) and moduli ratio (E_1/E_2) on the frequency response are investigated and the results are shown in Figs. 5(a) and 5(b), respectively. Fig. 5(a) shows that the backbone curves(which represent the relation between the free-vibration amplitude and the natural frequency) of different length-to-thickness ratios are the same, which means that there is not any change in the degree of hardening nonlinearity for different length-to-thickness ratios. Moreover, it is seen that when the length-to-thickness ratio increases, the frequency response curves bends away from the$\sigma/\omega_L = 0$ axis.It is seen from Fig. 5(b) that the higher is moduli ratio, the greater are the coefficients of nonlinear terms in the equation of motion (i.e., Eq. (17)), and subsequently frequency response curves bends away more from the $\sigma/\omega_L = 0$. In Figs. 5(c) and 5(d) the frequency responses of five-layered Glare 3 and Glare 5 square plates are compared for h = 1.4 mm, while the thickness of all GFRC layers are 0.1 mm. The layup of Glare 5 plate is in the following form (Botelho et al., 2006):

Al (2024-T3) / [0°/90°/90°/0°] GFRC / Al (2024-T3) / [0°/90°/90°/0°] GFRC / Al (2024-T3).

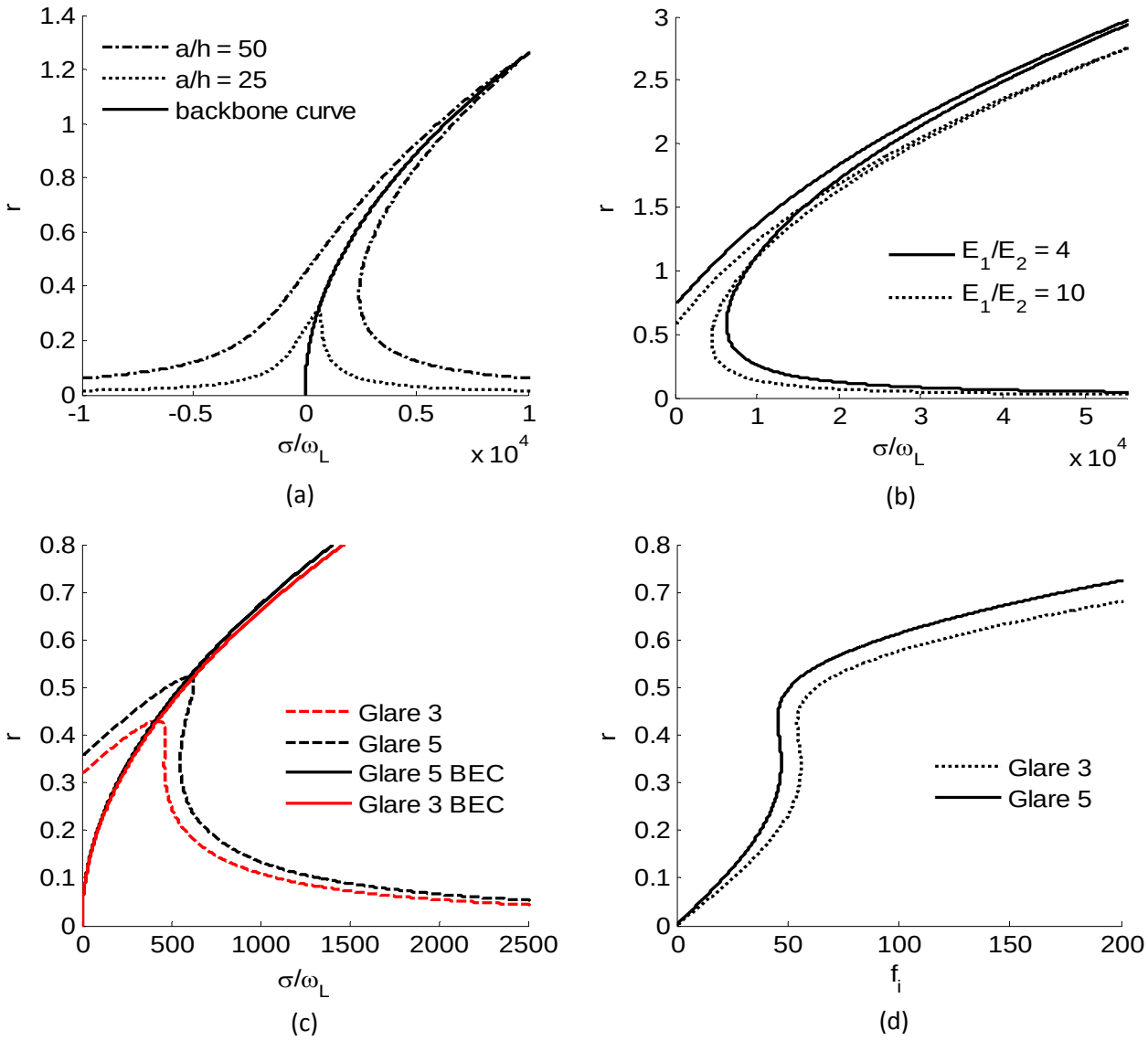

Fig. 5. Frequency response curve of a three-layered GFRC for: (a) two a/h ratios, ($f_i = 72.8$), and (b) two E_1/E_2 ratios, ($f_i = 72.8$). (c) Frequency response curve for five-layered square Glare 3 and Glare 5 plates ($f_i = 52$ and BEC stands for backbone curve), and (d) amplitude of the response as a function of amplitude of the excitation for five-layered square Glare 3 and Glare 5 plates, ($\sigma/\omega_L = 500$), and for all cases $\xi = 0.05$

Fig. 6 shows the effects of several parameters on the variation of the amplitude of response in terms of the excitation amplitude, which is called amplitudes curve hereafter for brevity. The jump phenomenon only occurs at excitation frequencies, which are greater than natural frequencies of plates. For example, for a five-layered Glare 3 square plate, $\sigma/\omega_L > 0$causes jump in the amplitudes curvewhich is shown in Fig. 6(a). The amplitudes curves of five-layered Glare 3 and GFRC square plates are compared with each other and shown in Fig. 6(b). As it is predictable, it is noticed that by increasing the excitation amplitude, the response amplitude of the GFRC plate increases with higher rate. It is seen from Fig. 6(c) that for higher aspect ratios, by increasing the excitation amplitude, the response amplitude increases with lower rate.

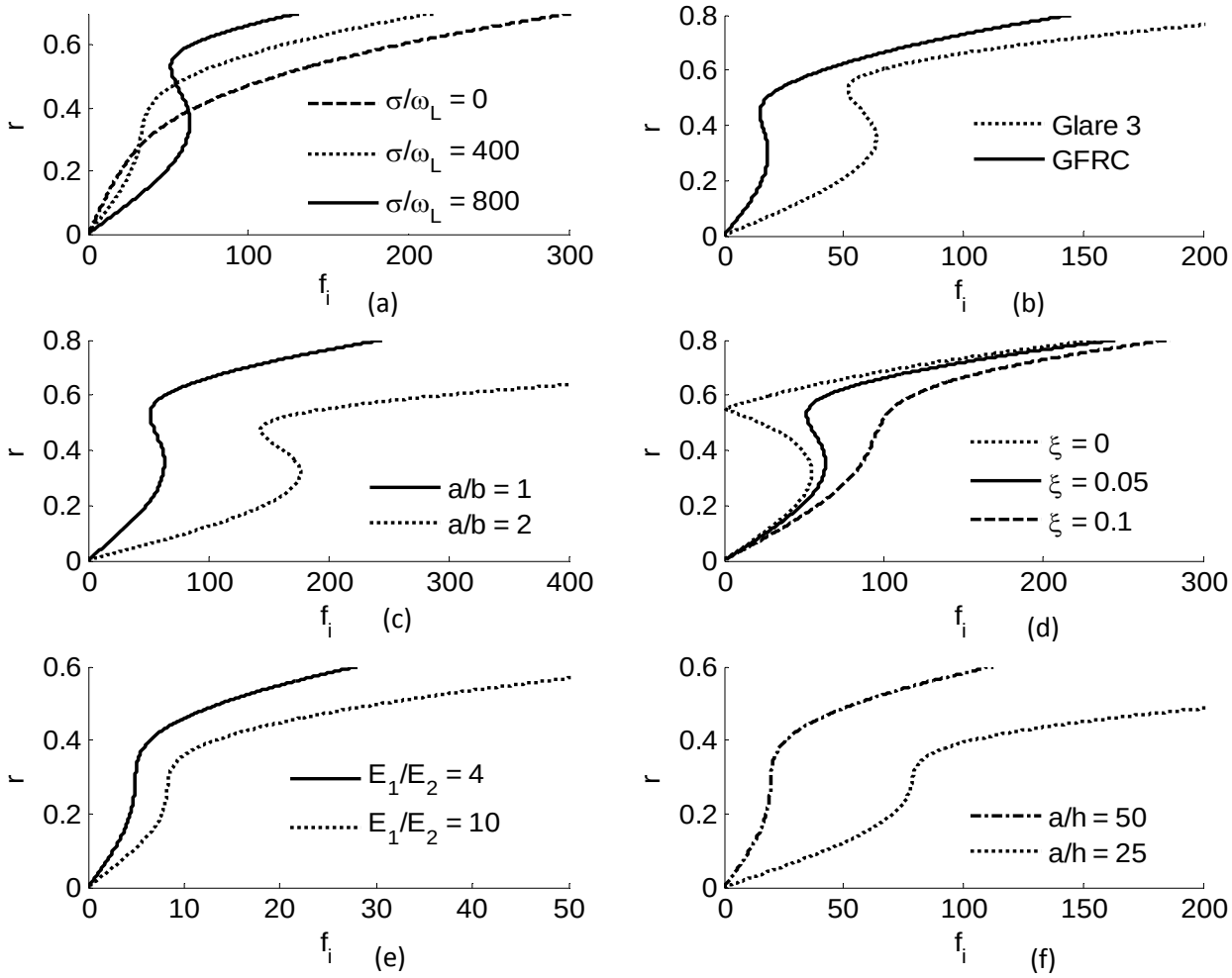

Fig. 6. Variation of the amplitude of response with respect to the excitation amplitude (amplitudes curve) of: (a) a square Glare 3 plate for different excitation frequencies ($\xi = 0.05$), (b) two different square plates ($\xi = 0.05$), (c) a square Glare 3 plate for two aspect ratios ($\xi = 0.05$), (d) a square Glare 3 for three different damping ratios, (e) two three-layered GFRC plates with different moduli ratios ($\xi = 0.05$), and (f) two three-layered GFRC plates with different aspect ratios ($\xi = 0.05$)

Fig. 6 shows the effects of several parameters on the variation of the amplitude of response in terms of the excitation amplitude, which is called amplitudes curve hereafter for brevity. The jump phenomenon only occurs at excitation frequencies, which are greater than natural frequencies of plates. For example, for a five-layered Glare 3 square plate, $\sigma/\omega_L > 0$causes jump in the amplitudes curvewhich is shown in Fig. 6(a). The amplitudes curves of five-layered Glare 3 and GFRC square plates are compared with each other and shown in Fig. 6(b). As it is predictable, it is noticed that by increasing the excitation amplitude, the response amplitude of the GFRC plate increases with higher rate. It is seen from Fig. 6(c) that for higher aspect ratios, by increasing the excitation amplitude, the response amplitude increases with lower rate. Fig. 6(d) shows that for un-damped rectangular plates, one of the bifurcation points is located on the *r*-axis indicating that the response amplitude never decays during vibration. The effects of moduli ratio on the amplitudes curve is similar to the effect of aspect ratio on this curve which can be noticed by comparing the curves of Figs. 6(c) and 6(e).Fig. 6(f) shows that for rectangular plates with higher length-to-thickness ratios (a/h), the response amplitude is larger for specific excitation amplitude. Equation of motion in time domain (i.e., Eq. (17)) is solved numerically for a five-layered Glare 3 square plate by using the Rung-Kutta method.

The numerical solution is compared with the analytical solution (i.e., Eq. (33)) and shown in Fig. 7. It is observed that there is a good agreement between the numerical and analytical solutions of nonlinear ordinary equation of motion.

5.2 Super-harmonic resonance

The effects of various parameters on the frequency responses of laminated rectangular plates are investigated and the results are shown in Fig. 8. The number of layers has negligible effect on the frequency response of laminated rectangular plates. This is shown in Fig. 8(a). Fig.8(b) shows that Glare 2B and Glare 3 plates have almost the same frequency response curves, but unlike the primary

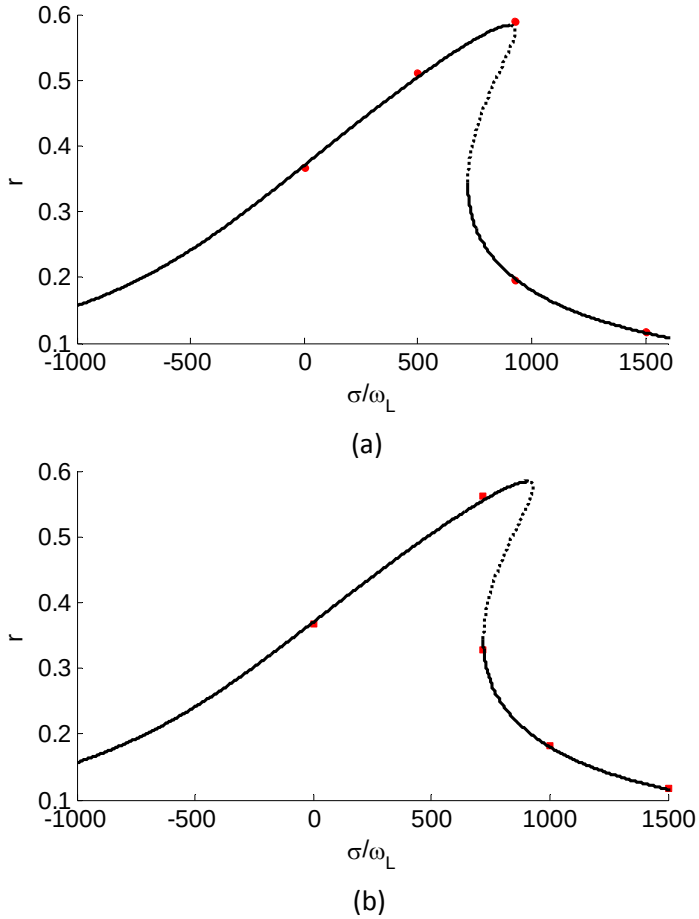

Fig. 7. Comparison of numerical solution with analytical solution: (a) when increasing excitation frequency, and (b) when decreasing excitation frequency for a five-layered square Glare 3.———— stable, -------- unstable, •&▪ numerical

resonance, in the super-harmonic resonance the Glare 4B plate has smaller peak amplitude than the peak amplitudes of Glare 2B and Glare 3 plates. It is seen from Fig. 8(c) that for higher excitation amplitudes, the frequency response curves bend away more from the vertical axis and unstable region occurs at larger detuning parameters. The effects of the aspect ratio on the frequency response curve are shown in Fig. 8(d). It is noticed that by increasing the aspect ratio, the degree of hardening nonlinearity and the peak amplitude decrease. Fig. 8(e) shows the effect of moduli ratio on the frequency response of a five-layered GFRC square plate. It is observed that for higher moduli ratios, the peak amplitude decreases. The comparison between numerical and analytical solutions is also done and shown in Fig. 8(f) in which it is seen that there is a good agreement between them.

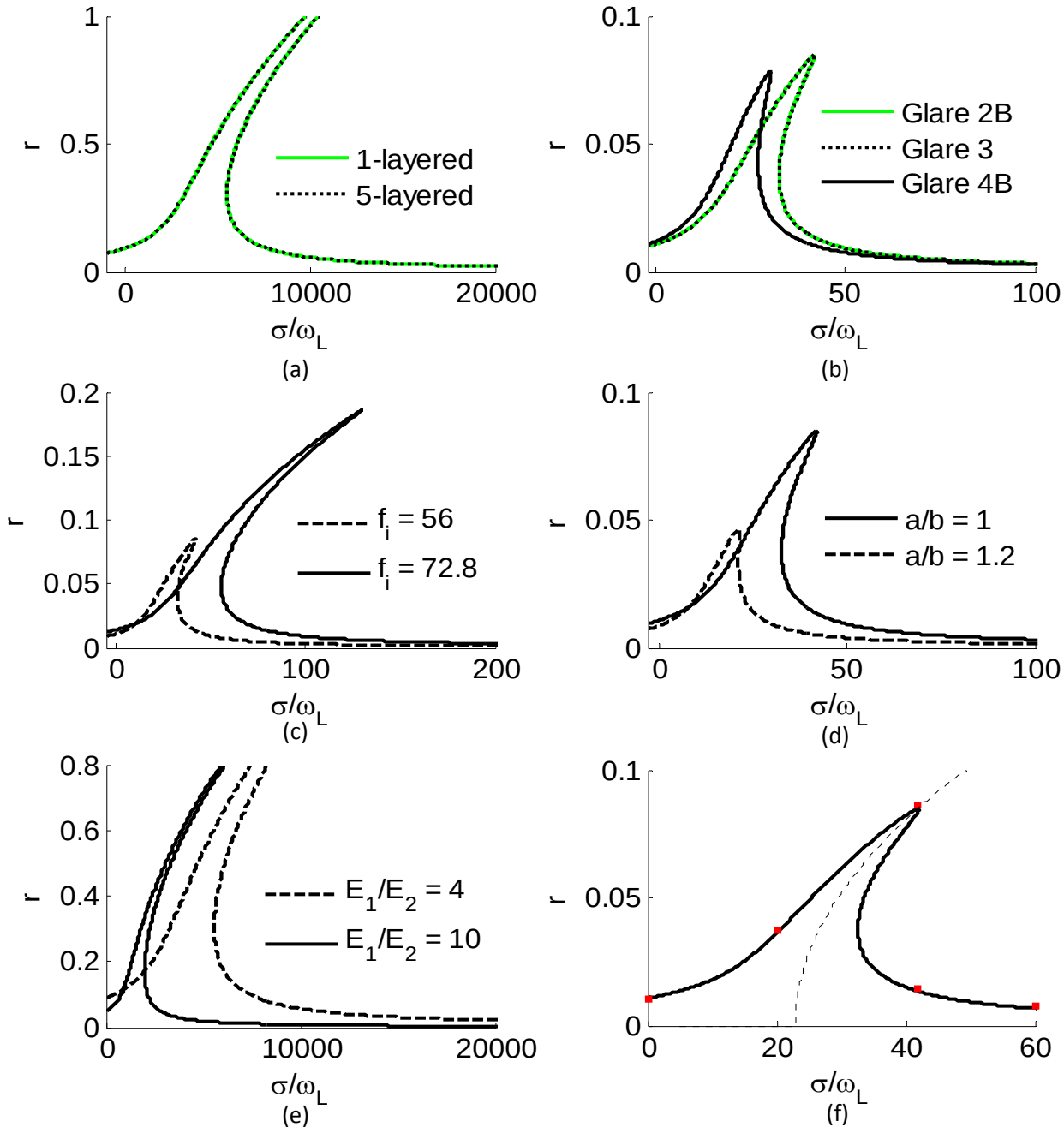

Fig. 8. Frequency response curve of: (a) two square GFRC plates with different number of layers ($f_i = 72.8$), (b) several five-layered square Glare plates ($f_i = 56$), (c) a five-layered square Glare 3 plate for different excitation amplitudes, (d) a five-layered rectangular Glare 3 plate for different aspect ratios ($f_i = 56$), (e) a five-layered square GFRC plate for different moduli ratios ($f_i = 72.8$), and (f) a five-layered square Glare 3 plate with numerical solution compared with it ($f_i = 56$), and for all cases $\xi = 5 \times 10^{-4}$

It is seen from Fig. 9 that after the jump, the amplitude of the response decreases firstly. Then it increases as the amplitude of the excitation increases. This can also be seen by comparing Eq. (33) with Eq. (43); in Eq. (43) there is an extra term multiplying the amplitude(r), $P_1\tilde{Q}^2$.As f_i is increased for specificσ/ω_L, the effect is to decrease the apparent detuning. Thus when f_i increases, there are two influences competing simultaneously: one tends to increase the amplitude of the response while

the other tends to decrease the amplitude of the response (Nayfeh & Mook, 1995). The effects of the

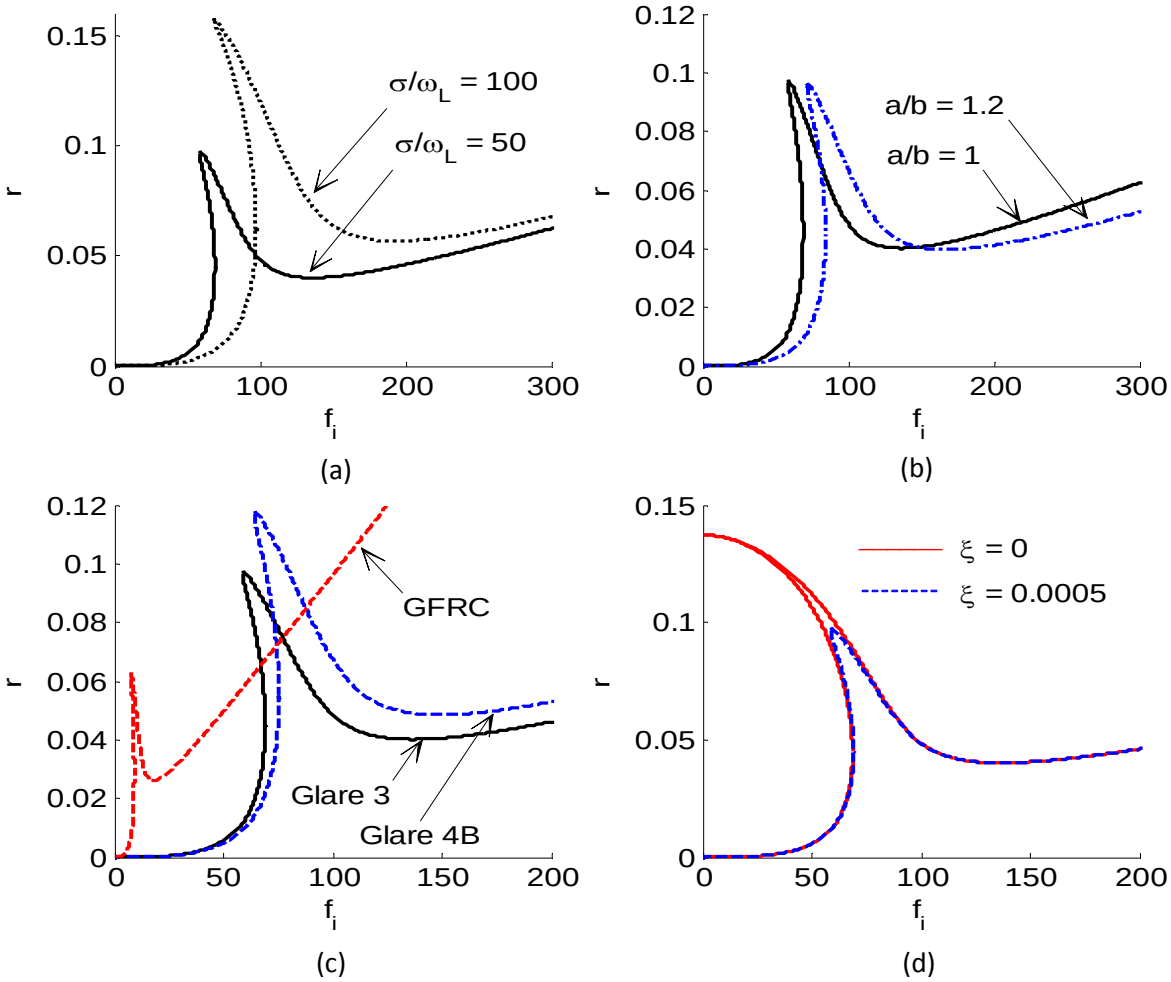

Fig. 9. Variation of the amplitude of response with respect to the excitation amplitude (amplitudes curve) of a five-layered: (a) square Glare 3 plate for different σ/ω_L ratios ($\xi = 0.0005$), (b) a rectangular Glare 3 plate for two aspect ratios ($\sigma/\omega_L = 50, \xi = 0.0005$), (c) square Glare 3 plate compared with the Glare 4B and GFRC plates ($\sigma/\omega_L = 50, \xi = 0.0005$), and (d) square Glare 3 plate for undamped and damped cases ($\sigma/\omega_L = 50$)

excitation frequency on the amplitudes curve are shown in Fig. 9(a). Fig. 9(b) shows that after initial decrease, the response amplitude of lower aspect ratios increases with higher rate. It is also seen that jump phenomenon in plates with lower aspect ratios occurs at smaller amplitudes of excitation. It can be understood from Fig. 9(c) that the jump phenomenon in the GFRC plate occurs in smaller excitation amplitudes comparing with the Glare 3 and Glare 4B plates. Therefore, GFRC plate reaches unstable region in smaller excitation amplitudes. Fig. 9(d) shows that changing of the damping ratio only changes the locus of one of bifurcation points. It is seen that for $\xi = 0$, this point is located on the r-axis, meaning that the plate continues to vibrate in the un-damped case even after elimination of the external force.

5.3 Sub-harmonic resonance

The effects of several parameters on the frequency response of laminated rectangular plates are investigated and the results are shown in Fig. 10. Similar to primary and super-harmonic resonances, the number of layers has negligible effect on the frequency response curve, which is shown in Fig. 10(a). Fig. 10(b) shows that the frequency responses of the Glare 2B and Glare 3 rectangular plates are almost the same. Fig. 10(c) shows the effects of excitation amplitude on the frequency response of laminated rectangular plates in which it is seen that for higher excitation amplitudes, smaller

excitation frequencies are needed to have a steady-state motion. It is seen from Fig. 10(d) that for lower aspect ratios, smaller excitation frequencies are needed to have a steady-state motion. Fig. 10(e) shows that for higher moduli ratios response amplitude increases with lower rate. Numerical and analytical solutions of nonlinear ordinary differential equation of motion are compared with each other and the results are shown in Fig. 10(f).

6. Conclusion

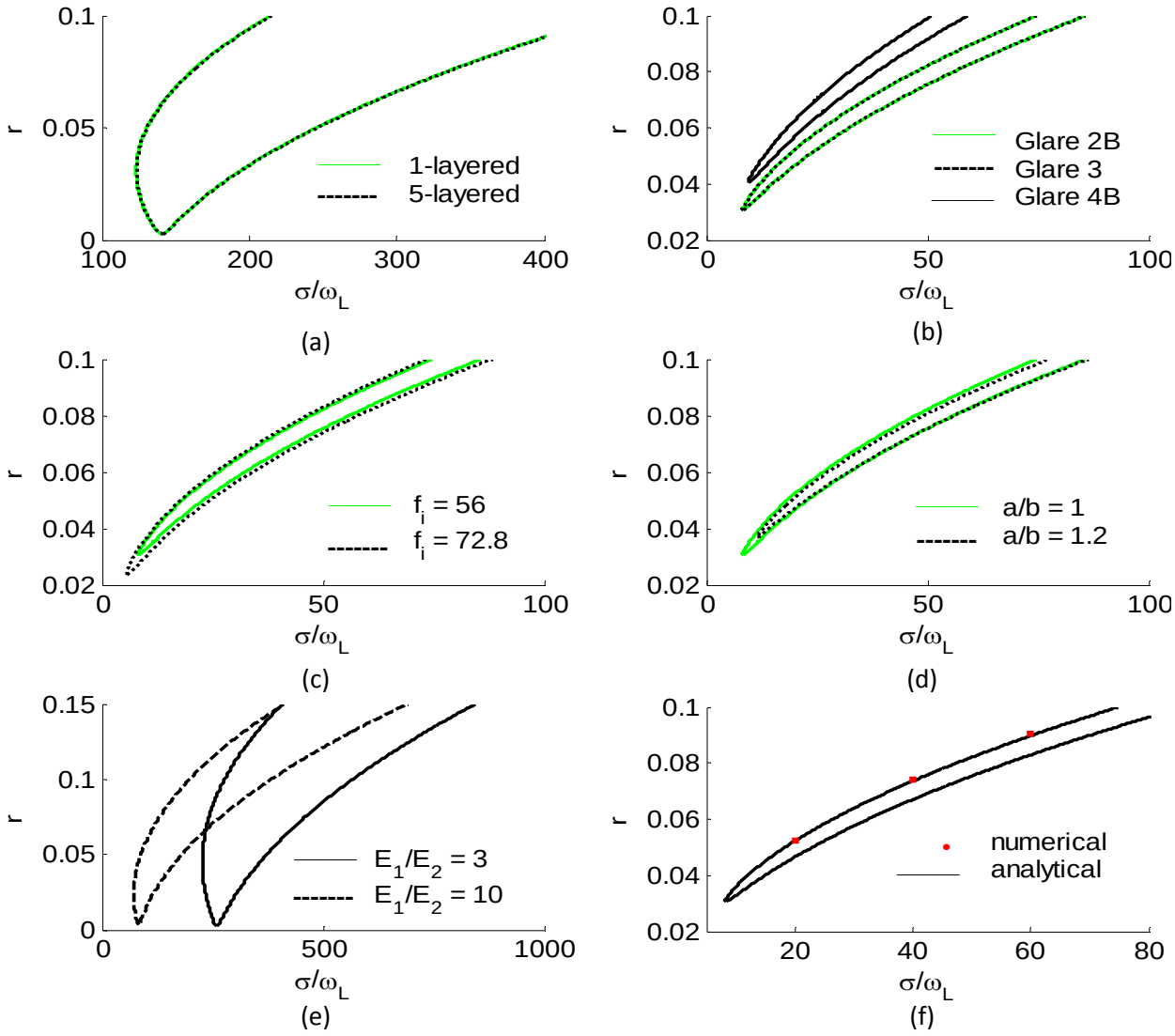

Fig. 10. Frequency response curve of: (a) two square GFRC plates with different number of layers ($f_i = 72.8$), (b) three grades of five-layered square Glare plate ($f_i = 56$), (c) a five-layered square Glare 3 plate under different excitation amplitudes, (d) two five-layered rectangular Glare 3 plate with different aspect ratios ($f_i = 56$), (e) two square GFRC plates with different moduli ratios ($f_i = 72.8$), and (f) a five-layered square Glare 3 plate compared with the numerical solution ($f_i = 56$), where for all cases $\xi = 10^{-4}$

Nonlinear forced vibration of symmetric laminated composite and Glare rectangular plates, with immovable simply supported boundary conditions is studied analytically by using the first order shear deformation theory, Galerkin method, and the method of multiple scales. The frequency response equations in steady-state motion of primary and secondary resonances are obtained. The effects of lamination parameters and plate properties on the steady-state motion of symmetric rectangular plates

are investigated. It is seen that the number of layers and layup scheme have negligible effects on the frequency response of symmetric rectangular plates. It is also apparent that due to the presence of aluminum layers in Glare plates, these plates have smaller response amplitudes comparing with the same-sized GFRC plates.

References

Abe, A., Kobayashi, Y.,& Yamada, G. (1998). Analysis of sub-harmonic resonance of moderately thick anti-symmetric angle-ply laminated plates by using method of multiple scales.*Journal of Sound and Vibration*,217(3), 467-484.

Amabili, M. (2004). Nonlinear vibrations of rectangular plates with different boundary conditions: theory and experiments. *Computers and Structures*, 82, 2587-2605.

Amabili, M., & Farhadi, S. (2009).Shear deformable versus classical theories for nonlinear vibrations of rectangular isotropic and laminated composite plates. *Journal of Sound and Vibration*, 320, 649-667.

Botelho, E. C., Silva, R. A., Pardini, L. C., & Rezende, M. C. (2006).A review on the development and properties of continuous fiber/epoxy/aluminum hybrid composites for aircraft structures.*Materials Research*, 9(3), 247-256.

Boumediene, F., Miloudi, A., Cadou, J. M., Duigou, L., & Boutyour, E. H. (2009). Nonlinear forced vibration of damped plates by an asymptotic numerical method. *Computers and Structures*, 87, 1508-1515.

Chia, C. Y. (1980). *Nonlinear Analysis of Plates*. McGraw-Hill.

Harras, B., Benamar, R., & White, R. G. (2002).Experimental and theoretical investigation of the linear and non-linear dynamic behaviour of a glare 3 hybrid composite panel. *Journal of Sound and Vibration*, 252(2), 281-315.

Langdon, G. S., Chi, Y., Nurick, G.N., & Haupt, P. (2009). Response of GLARE panels to blast loading. *Engineering Structures*, 31(12), 3116-3120.

Lu H. X., & Li J. Y. (2009). Analysis of an initially stressed laminated plate based on elasticity theory. *Composite Structures*, 88, 271-279.

Nayfeh, A. H., &Mook, D. T. (1995).*Nonlinear Oscillation*. John Wiley & Sons, Inc.

Rashidi, M. M., Shooshtari, A., & Anwar Bég, O. (2012). Homotopy perturbation study of nonlinear vibration of Von Karman rectangular plates. *Computers and Structures*, 106-107, 46-55.

Reddy, J. N. (2004).*Mechanics of laminated composite plates and shells: theory and analysis*. second ed. CRC Press.

Ribeiro, P. (2004). Non-linear forced vibrations of thin/thick beams and plates by the finite element and shooting methods. *Computers and Structures*, 82, 1413-1423.

Ribeiro, P. (2005). Nonlinear vibrations of simply-supported plates by the *p*-version finite element method. *Finite Elements in Analysis and Design*, 41, 911-924.

Ribeiro, P. (2006). Forced periodic vibrations of laminated composite plates by a p-version, first order shear deformation, finite element. *Composites Science and Technology*, 66, 1844-1856.

Ribeiro, P. (2009). On the influence of membrane inertia and shear deformation on the geometrically nonlinear vibrations of open, cylindrical, laminated clamped shells. *Composites Science and Technology*, 69, 176-185.

Shooshtari, A., & Razavi, S. (2010). A closed form solution for linear and nonlinear free vibrations of composite and fiber metal laminated rectangular plates. *Composite Structures*, 92, 2663-2675.

Singha, M. K., & Daripa, R. (2009).Nonlinear vibration and dynamic stability analysis of composite plates. *Journal of Sound and Vibration*, 328, 541-554.

Wei, C. L., Chen, C. S., Shih, C. S., & Chang, Y. C. (2012). Nonlinear vibration of initially stressed hybrid composite plates on elastic foundations. *Mechanics of Composite Materials*, 48(4), 467-482.

Zhang, W., & Zhao, M. H. (2012). Nonlinear vibrations of a composite laminated cantilever rectangular plate with one-to-one internal resonance. *Nonlinear Dynamics*, 70(1), 295-313.

Appendix A

$$L_1^* = D_{11}\frac{\partial^2}{\partial x^2} + D_{66}\frac{\partial^2}{\partial y^2} - I_2\frac{\partial^2}{\partial t^2} - KA_{55} \tag{A.1}$$

$$L_2^* = L_4^* = (D_{12} + D_{66})\frac{\partial^2}{\partial x \partial y} \tag{A.2}$$

$$L_3^* = KA_{55}\frac{\partial}{\partial x} \tag{A.3}$$

$$L_5^* = D_{66}\frac{\partial^2}{\partial x^2} + D_{22}\frac{\partial^2}{\partial y^2} - I_2\frac{\partial^2}{\partial t^2} - KA_{44} \tag{A.4}$$

$$L_6^* = KA_{44}\frac{\partial}{\partial y} \tag{A.5}$$

Appendix B

$$\begin{aligned} Z_1 = \frac{-h}{4a^3b^3}\Big\{ & I_0\left(\pi^4 D_{22}D_{66}a^4 + \pi^2 KA_{44}D_{66}b^2a^4 + b^4\pi^4 D_{66}D_{11} + \pi^2 KA_{55}D_{22}b^2a^4\right. \\ & \pi^2 KA_{44}D_{11}a^2b^4 - \pi^4 D_{12}^2 b^2a^2 + K^2A_{44}A_{55}b^4a^4 + \pi^4 D_{22}D_{11}b^2a^2 \\ & \left. -2\pi^4 D_{66}D_{12}b^2a^2 + \pi^2 KA_{55}D_{66}a^2b^4\right) \\ & I_2K\left(\pi^4 A_{44}D_{66}a^2\left(a^2+b^2\right) + \pi^4 A_{55}D_{22}b^2a^2 + \pi^4 A_{44}D_{11}b^2a^2 + \right. \\ & \pi^4 A_{55}D_{11}b^4 + \pi^2 KA_{44}A_{55}a^2b^2\left(a^2+b^2\right) + \pi^4 A_{55}D_{66}b^2\left(a^2+b^2\right) \\ & \left. + \pi^4 A_{44}D_{22}a^4\right)\Big\} \end{aligned} \tag{B.1}$$

$$\begin{aligned} Z_2 = \frac{-Kh\pi^4}{4a^5b^5}\Big\{ & \pi^2\left(A_{55}b^6D_{66}D_{11} + A_{44}a^6D_{22}D_{66} + A_{55}b^2a^4D_{22}D_{66} + A_{44}D_{22}D_{11}a^4b^2\right. \\ & A_{55}b^4D_{22}D_{11}a^2 - A_{44}a^4D_{12}^2b^2 + A_{44}a^2b^4D_{66}D_{11} - A_{55}b^4D_{12}^2a^2 \\ & \left. -2A_{55}b^4D_{66}D_{12}a^2 - 2A_{44}a^4D_{66}D_{12}b^2\right) + KA_{44}A_{55}a^2b^2\left(4b^2a^2D_{66} + \right. \\ & \left. 2a^2b^2D_{12} + b^4D_{11} + a^4D_{22}\right)\Big\} \end{aligned} \tag{B.2}$$

$$\begin{aligned} Z_3 = \frac{-\pi^4h^3}{64b^7a^7A_{22}A_{11}}\Big\{ & \left(-A_{12}^2a^4A_{22} + 3A_{22}^2a^4A_{11} - A_{12}^2b^4A_{11} + 4A_{12}a^2b^2A_{11}A_{22} + 3A_{11}^2b^4A_{22}\right) \\ & \times\left(a^4\pi^2 KA_{55}D_{22}b^2 + a^4K^2A_{44}A_{55}b^4 + a^4\pi^4 D_{22}D_{66} + a^4\pi^2 KA_{44}D_{66}b^2\right. \\ & -a^2\pi^4 D_{12}^2b^2 - 2a^2\pi^4 D_{66}D_{12}b^2 + a^2\pi^2 KA_{44}D_{11}b^4 + a^2\pi^2 KA_{55}D_{66}b^4 \\ & \left. + a^2\pi^4 D_{22}D_{11}b^2 + \pi^4 D_{66}D_{11}b^4\right)\Big\} \end{aligned} \tag{B.3}$$

$$\begin{aligned} Z_4 = \frac{-3\pi^4h^3I_2}{64b^5a^5A_{22}A_{11}}\Big\{ & \left(-A_{12}^2a^4A_{22} + 3A_{22}^2a^4A_{11} - A_{12}^2b^4A_{11} + 4A_{12}a^2b^2A_{11}A_{22} + 3A_{11}^2b^4A_{22}\right) \\ & \times\left(a^2\pi^2\left(D_{22}+D_{66}\right) + a^2b^2K\left(A_{44}+A_{55}\right) + b^2\pi^2\left(D_{11}+D_{66}\right)\right)\Big\} \end{aligned} \tag{B.4}$$

$$\begin{aligned} Z_5 = \frac{-3\pi^4h^3I_2}{32b^5a^5A_{22}A_{11}}\Big\{ & \left(-A_{12}^2a^4A_{22} + 3A_{22}^2a^4A_{11} - A_{12}^2b^4A_{11} + 4A_{12}a^2b^2A_{11}A_{22} + 3A_{11}^2b^4A_{22}\right) \\ & \times\left(a^2\pi^2\left(D_{22}+D_{66}\right) + a^2b^2K\left(A_{44}+A_{55}\right) + b^2\pi^2\left(D_{11}+D_{66}\right)\right)\Big\} \end{aligned} \tag{B.5}$$